Supplemental Material:
TMDs as a platform for spin liquid physics: A strong coupling study of twisted bilayer WSe_2

I. CLASSICAL MONTE CARLO RESULTS FOR INCOMMENSURATE PHASES

In Fig. 1(a) and (b) we show classical Monte Carlo results for the incommensurate phases, ICS-I and ICS-II (as mentioned in the main text, ICS-III can be generated from ICS-I via a three-sublattice transformation). The spins are coplanar within the xy-plane and the static spin structure factor exhibits four peaks, at $\pm\mathbf{k}_1$ and $\pm\mathbf{k}_2$, with $\mathbf{k}_1, \mathbf{k}_2$ being incommensurate. The Monte Carlo results clearly indicate that the Luttinger-Tisza ordering wavevectors are indeed correct.

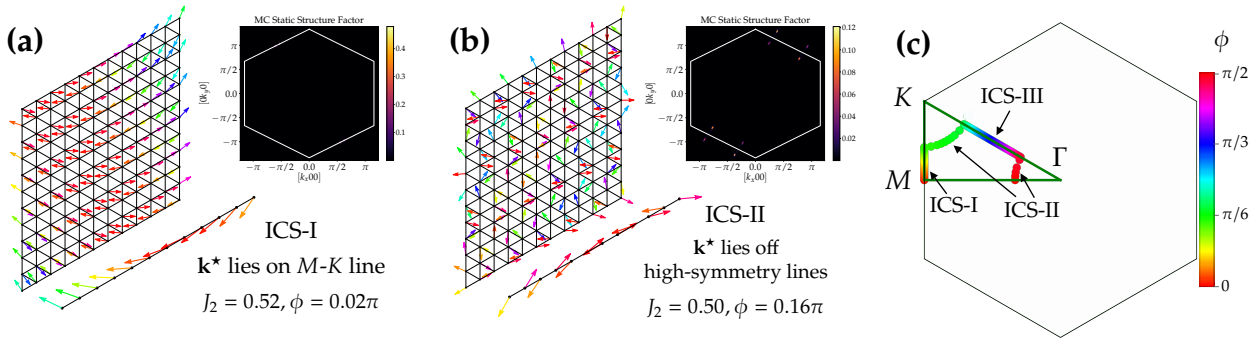

FIG. 1. **Classical Monte Carlo results** for (a) the ICS-I phase and (b) the ICS-II phase. In both cases, we show a portion of the low-temperature spin configurations in real space (12×12 and 12×1 examples out of a total of 96×96 spins), as well as the static structure factor in momentum space (unfortunately the sharpness of the structure factor peaks makes them somewhat difficult to see). Since both phases exhibit ordering within the xy-plane we show only the xy-components, and, to help in making the patterns more visible, we artificially color the spins according to the value of their x component. In (c), we show the predicted Luttinger-Tisza ordering wavevectors, only within the area enclosed by the high-symmetry lines, for $J_2 = 0.5$ and $\phi \in [0, \pi/2]$. The regions corresponding to the three incommensurate phases, ICS-I, II and III are marked, and the color indicates the value of ϕ.

II. PSEUDO-FERMION FUNCTIONAL RENOMALIZATION GROUP

In this section, further technical details of the pf-FRG approach are discussed. As already mentioned in the main text, the hierarchy of differential equations at the heart of the FRG method has to be truncated to allow for a numerical solution. Within the Katanin truncation, the single-scale propagator $S^\Lambda \equiv -\frac{d}{d\Lambda} G^\Lambda|_{\Sigma^\Lambda = \text{const.}}$ is replaced by a full derivative of the dressed propagator G^Λ to partially include certain diagrammatic contributions of the three-particle vertex in the two-particle vertex flow. The flow equations for the self energy Σ^Λ and the two-particle vertex Γ^Λ then read

$$\frac{d}{d\Lambda}\Sigma^\Lambda(1) = -\frac{1}{2\pi}\sum_2 \Gamma^\Lambda(1,2;1,2)S^\Lambda(2) \tag{1}$$

$$\frac{d}{d\Lambda}\Gamma^{\Lambda}(1',2';1,2) = \frac{1}{2\pi}\sum_{3,4}\big[\Gamma^{\Lambda}(3,4;1,2)\Gamma^{\Lambda}(1',2';3,4) - \Gamma^{\Lambda}(1',4;1,3)\Gamma^{\Lambda}(3,2';4,2) - (3\leftrightarrow 4) + \Gamma^{\Lambda}(2',4;1,3)\Gamma^{\Lambda}(3,1';4,2) + (3\leftrightarrow 4)\big] \times G^{\Lambda}(3)\bigg(-\frac{d}{d\Lambda}G^{\Lambda}(4)\bigg), \tag{2}$$

where multi-indices comprise a lattice, spin and frequency argument, e.g. $1 = (i_1, \alpha_1, w_1)$. The flow equations can be further simplified by exploiting symmetries in real and spin space, as well as in the Matsubara frequencies. Since these simplifications are extensively discussed in Ref. 1, we only state the most important results here. Firstly, for time-reversal symmetric Hamiltonians, all one particle objects are diagonal in their indices and only depend on one frequency argument. Note, that this property has already been used to simplify (1) and (2) and the self energy, for example, should be regarded as

$$\Sigma(1) = \Sigma(w_1) \tag{3}$$

where $\Sigma(w) = -i\gamma(w)$ is purely imaginary and anti-symmetric in frequency space. The two particle vertex, on the other hand, is a bi-local object with purely real and purely imaginary components that encode the spin interaction of the respective Hamiltonian. For our model, we may write

$$\begin{aligned}\Gamma(1',2';1,2) = \Big[&\Gamma^{\mathrm{XX}}_{i_{1'}i_{2'}}(w_{1'},w_{2'},w_1)\times(\sigma^x_{\alpha_{1'}\alpha_1}\sigma^x_{\alpha_{2'}\alpha_2}+\sigma^y_{\alpha_{1'}\alpha_1}\sigma^y_{\alpha_{2'}\alpha_2})\\ &+\Gamma^{\mathrm{ZZ}}_{i_{1'}i_{2'}}(w_{1'},w_{2'},w_1)\times\sigma^z_{\alpha_{1'}\alpha_1}\sigma^z_{\alpha_{2'}\alpha_2}\\ &+\Gamma^{\mathrm{DM}}_{i_{1'}i_{2'}}(w_{1'},w_{2'},w_1)\times(\sigma^x_{\alpha_{1'}\alpha_1}\sigma^y_{\alpha_{2'}\alpha_2}-\sigma^y_{\alpha_{1'}\alpha_1}\sigma^x_{\alpha_{2'}\alpha_2})\\ &+\Gamma^{\mathrm{DD}}_{i_{1'}i_{2'}}(w_{1'},w_{2'},w_1)\times\delta_{\alpha_{1'}\alpha_1}\delta_{\alpha_{2'}\alpha_2}\\ &+i\Gamma^{\mathrm{ZD}}_{i_{1'}i_{2'}}(w_{1'},w_{2'},w_1)\times\sigma^z_{\alpha_{1'}\alpha_1}\delta_{\alpha_{2'}\alpha_2}\\ &+i\Gamma^{\mathrm{DZ}}_{i_{1'}i_{2'}}(w_{1'},w_{2'},w_1)\times\delta_{\alpha_{1'}\alpha_1}\sigma^z_{\alpha_{2'}\alpha_2}\Big]\times\delta_{i_{1'}i_1}\delta_{i_{2'}i_2}\delta(w_{1'}+w_{2'}-w_1-w_2)-(1'\leftrightarrow 2').\end{aligned} \tag{4}$$

The initial conditions for the flow equations then read

$$\begin{aligned}\gamma^{\Lambda\to\infty}(w) &= 0\\ \Gamma^{\mathrm{XX}\,\Lambda\to\infty}_{i_{1'}i_{2'}}(w_{1'},w_{2'},w_1) &= \frac{J_1}{4}\cos(2\phi_{i_{1'}i_{2'}})\times\mathbf{1}_{\langle i_{1'}i_{2'}\rangle}+\frac{J_2}{4}\times\mathbf{1}_{\langle\langle i_{1'}i_{2'}\rangle\rangle}\\ \Gamma^{\mathrm{ZZ}\,\Lambda\to\infty}_{i_{1'}i_{2'}}(w_{1'},w_{2'},w_1) &= \frac{J_1}{4}\times\mathbf{1}_{\langle i_{1'}i_{2'}\rangle}+\frac{J_2}{4}\times\mathbf{1}_{\langle\langle i_{1'}i_{2'}\rangle\rangle}\\ \Gamma^{\mathrm{DM}\,\Lambda\to\infty}_{i_{1'}i_{2'}}(w_{1'},w_{2'},w_1) &= \frac{J_1}{4}\sin(2\phi_{i_{1'}i_{2'}})\times\mathbf{1}_{\langle i_{1'}i_{2'}\rangle}\\ \Gamma^{\mathrm{DD}\,\Lambda\to\infty}_{i_{1'}i_{2'}}(w_{1'},w_{2'},w_1) &= 0\\ \Gamma^{\mathrm{ZD}\,\Lambda\to\infty}_{i_{1'}i_{2'}}(w_{1'},w_{2'},w_1) &= 0\\ \Gamma^{\mathrm{DZ}\,\Lambda\to\infty}_{i_{1'}i_{2'}}(w_{1'},w_{2'},w_1) &= 0,\end{aligned} \tag{5}$$

where, for example, $\mathbf{1}_{\langle ij\rangle}$ is should be understood as

$$\mathbf{1}_{\langle ij\rangle} = \begin{cases}1 \text{ if i and j are nearest-neighbors}\\ 0 \text{ else}\end{cases} \tag{6}$$

For our work, we extend the open-source Julia package `PFFRGSolver.jl`[2], which provides a state-of-the-art pf-FRG solver for various lattice structures. We use a set of $N_\Sigma = 500$ frequencies for the self energy and $N_\Gamma = 50\times 60$ transfer/fermionic frequencies to model the two-particle vertex. The lattice truncation is fixed to $L = 10$, i.e.

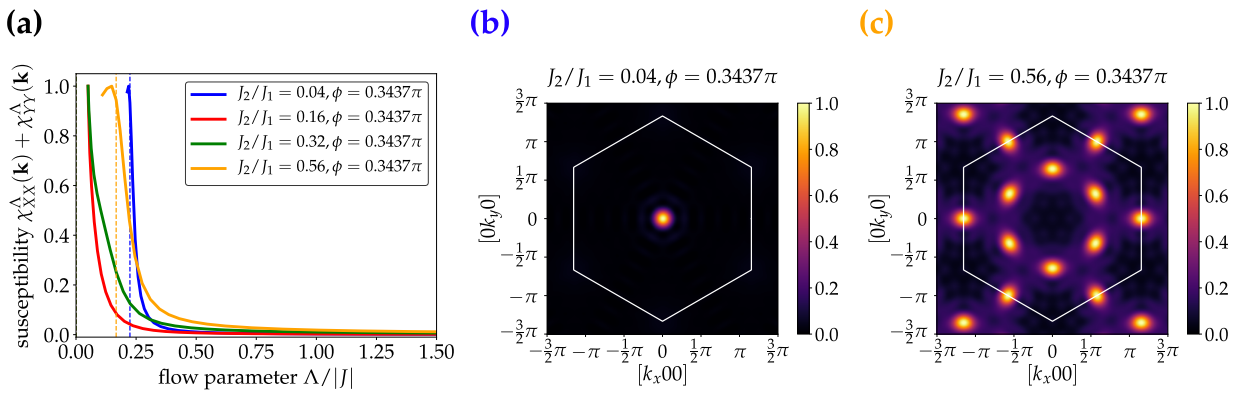

FIG. 2. **pf-FRG data at $\pi/3+\pi/96$.** In panel (a) we display representative RG flows, indicating, as expected from the considerations in Sec. II of the main text, a paramagnetic phase, quenched between the long-range ordered ferromagnetic (b) and stripe / type-III incommensurate phases (c). The incommensurate part of the correlation spectrum is generated by the in-plane correlations, where out-of-plane spin correlators χ^{Λ}_{ZZ} contribute the peaks at the M points (related to stripy long-range order).

correlations are set to zero beyond 10 bonds away from a given reference site. The accuracy for the involved integration routines has been set to $a_{\text{tol}}, r_{\text{tol}} = (10^{-5}, 10^{-3})$ for which our results were found to be well converged.
In principle, the RG flow should diverge, once symmetries of the Hamiltonian are spontaneously broken during the flow to strong coupling. However, due to the relaxed particle number constraint and finite numerical resolution, phases with strongly competing channels occasionally develop softened features such as pronounced shoulders. Reading off the precise value of the characteristic scale Λ_c in this case is rather difficult and a numerical criterion is needed to automate this process. Here, we utilize that the bare susceptibility $\chi^{\Lambda}_0(w=0) = \int_{-\infty}^{\infty} dv (G^{\Lambda}_0(v))^2 \sim 1/\Lambda$, where $G^{\Lambda}_0(v) = (1-e^{-v^2/\Lambda^2})/(iv)$ is the regularized bare propagator. Now, whenever the flow shows a distinct divergence or a sharp peak, we set Λ_c to the position of this respective feature. If the breakdown is more washed out, we instead determine the scale with the strongest concavity, i.e. the largest deviation from the expected behavior of the non-interacting, paramagnetic system. If none of these criteria apply and the flow remains convex and featureless, we classify the ground state as non-magnetic.

III. PF-FRG RESULTS FOR $\phi > \pi/6$

In this section we discuss numerical results beyond the $[0, \frac{\pi}{6}]$ range focused on in the main text. As discussed in Sec. II of the main text, one would expect the energy spectrum of our Hamiltonian to be repeated within periods of $\pi/3$. While the ground state wave function, and therefore the label of the respective phase, will generally change, the spin liquid region for which the characteristic energy scale Λ_c vanishes, should re-appear upon varying ϕ. To illustrate this circumstance we have summarized representative pf-FRG data for $\phi = \pi/3+\pi/96$ in Fig. 2. Indeed, smooth RG flows, indicating a paramagnetic ground state, are obtained within the expected J_2 range, accompanied by sharp flow breakdowns in the adjacent magnetic phases. For large J_2, our FRG approach implies the presence of another stripy state in coexistence with the nearby ICS-III phase as visible from Fig. 2(c), where Bragg peaks for both orders are visible. The incommensurate correlations are contributed by the in-plane, that is $\chi^{\Lambda}_{\text{XX/YY}}$, components of the susceptibility, whereas the peaks at the M-points steam from χ^{Λ}_{ZZ}.

[1] F. L. Buessen, V. Noculak, S. Trebst, and J. Reuther, "Functional renormalization group for frustrated magnets with nondiagonal spin interactions," Physical Review B **100** (2019), 10.1103/physrevb.100.125164.
[2] D. Kiese, T. Mueller, Y. Iqbal, R. Thomale, and S. Trebst, "Multiloop functional renormalization group approach to quantum spin systems," (2021), arXiv:2011.01269 [cond-mat.str-el].